Available online at www.sciencedirect.com

Manufacturing Letters

Manufacturing Letters 33 (2022) 109–116

50th SME North American Manufacturing Research Conference (NAMRC 50, 2022)

The Effect Of The Building Direction And Surface Finish On The Mechanical Properties Of The Direct Energy Deposited AISI 316L Stainless Steel

R. Bertolini[a]*, M. Perini[b], A. Ghiotti[a], S. Bruschi[a]

[a]*Dept. of Industrial Engineering, University of Padova, Via Venezia 1, 35131, Padova, Italy*
[b]*ProM Facility of Trentino Sviluppo, Rovereto, Italy*

* Corresponding author. Tel.: +39 049 8276819; fax: +39 049 8276819. E-mail address: rachele.bertolini@unipd.it

Abstract

Additive Manufacturing (AM) technologies, such as Direct Energy Deposition (DED) ones, offer new design possibilities for a wide range of industrial applications in different sectors. However, in order to widen the application fields, the knowledge of the mechanical behavior of AM parts is essential. The purpose of this paper is to investigate the effect of the building direction and surface finish on the static and dynamic mechanical properties of AISI 316L stainless steel specimens fabricated via DED. Samples were fabricated in their final shape through DED with the axis parallel to the building direction as well as prisms were fabricated from which samples with the axis oriented both vertically and horizontally with respect to the building direction were machined. Then, both the as-built and machined samples were characterized in terms of surface topography and microstructure as well as tensile and fatigue tested. Finally, the fracture surfaces were investigated.
Results showed that the horizontally machined samples were characterized by higher tensile strength than the vertically machined samples, since the load is parallel to the slide layers, which represent weakness points. On the contrary, it was proved that the surface finish plays the major role in increasing the fatigue resistance, as the fatigue limit of the machined samples was more than double than that of the as-built samples.

Keywords: Stainless steel, Additive Manufacturing, Direct Energy Deposition, Microstructure, Mechanical properties, Fatigue life

1. Introduction

During the last decade, Additive Manufacturing (AM) has gained increasing attention for the production not only of prototypes but also of functional parts to be put in service [1]. Laser Power Bed Fusion (LPBF) and Direct Energy Deposition (DED) are the most common AM techniques dedicated to metals, which, contrarily to traditional subtractive methods, build the part layer by layer thanks to the localized fusion of the metal powders by means of a laser. The two processes differ on the way in which the powders are fed, since in LPBF they are laid on the so-called "bed", whereas in DED they are continuously blown by one or multiple nozzles. Compared to LPBF, DED has the potentiality of manufacturing both functionally graded and single metal components, as well as it allows cladding worn pieces that could not be mended otherwise [2]. This significant flexibility makes DED applicable in many sectors, like aerospace, medical, and defense. Nevertheless, despite all the aforementioned advantages, the attainment of anisotropic microstructures and rough surfaces are the main weaknesses of both LPBF and DED. While the AM-induced microstructure anisotropy can be mitigated through heat treatments, the surface finish can be suitably modified through post-processing operations, like

machining operations, which can reduce AM-induced defects, like Lack of Fusion (LoF) or isolated porosities that may be present on the part external surfaces [3].

The anisotropic behavior in of the LPBF AISI 316L stainless steel was investigated in [4]. Tensile and compression tests, showed that severe anisotropy characterized the tensile data due to the anisotropic pore distribution. Similarly, the compression behavior showed differences in the Yield Strength (YS) and strain hardening on the basis of the loading direction. Similar results were found in [5] for the same LPBF AISI 316L where an increase of ∼10–20% in the YS and 12–13% in the Ultimate Tensile Stress (UTS) was recorded on samples fabricated with the axis at 45° with respect to the building direction compared to the samples with the axis at 90°, regardless of the laser power used for the LPBF process. Moreover, the elongation of samples built at 45° decreased by about 50% in comparison to those built at 90°. The anisotropic mechanical behavior of AISI 316L specimens fabricated via DED with horizontal, edge, and vertical axes in the with respect to the building direction was explored in [6]. Results showed that the tensile characteristics, namely YS, UTS and elongation to fracture, of the specimens built in the horizontal direction were noticeably higher, because the loading direction was parallel to the layer-by layer orientation. The influence of the surface quality on the high cycle fatigue strength was investigated in the case of AISI 316L specimens fabricated via LPBF [7]. Some as-built specimens were sandblasted whereas others were turned and then hand-polished. Results showed that polishing produced an improvement in the fatigue life, but the lifetime behaviour at high stress amplitudes was pretty similar to that of the as-built material.

The effect of milling and polishing operations on the rotary bending fatigue behavior of the LPBF Ti6Al4V titanium alloy was investigated in [8]. Results showed that these finishing operations were able to enhance the Ti6Al4V fatigue resistance compared to the as-built condition, rising it from 200 MPa to 250 MPa and 300 MPa for the polished and milled conditions, respectively. The influence of the microstructure and surface topography on the fatigue behavior of Ti6Al4V titanium alloy specimens produced by LPBF was evaluated in [9]. Four-point bending fatigue tests were performed on the top and side surfaces of samples produced with the same process parameters, which were, however, characterized by different topographies and microstructure. The texture of the specimen was characterized in terms of both areal reduced valley depth (Svk), which deals with the valley depth below the core roughness, and areal arithmetic mean height (Sa), which is the equivalent of Ra but calculated on a surface rather than a line. Results showed that the laser scanning track direction had a significant influence on the crack nucleation because it determined both the depth and orientation of the valleys that were quantified on the basis of the surface roughness parameters investigated. Authors found that the lower the Sa and Svk parameters the higher the fatigue strength.

Nevertheless, most of these studies lack of a comprehensive investigation of the mechanical properties, focusing either on the tensile or fatigue properties as representative of the AM metal mechanical behavior. Furthermore, few of them take into account the effect of the loading direction with respect to the specimen building direction, especially in the case of specimens fabricated through DED.

Therefore, in this framework, the aim of the work is to evaluate the influence of the building orientation and surface finish on the mechanical behavior of AISI 316L specimens fabricated through DED. First, the samples microstructure and surface finish were analyzed, and, afterwards, their mechanical performances evaluated making use of static and uniaxial fatigue tests. Finally, the fracture surfaces were analyzed to correlate the mechanical behaviour with the AM process-induced characteristics.

Nomenclature

As-built / Z	As-built sample with the axis parallel to the building direction Z
Machined / Z	Sample machined after DED with the axis parallel to the building direction Z
Machined / X	Sample machined after DED with the axis perpendicular to the building direction Z

2. Experimental procedure

2.1. Samples fabrication

AISI 316L gas atomized spherical powders, supplied by MIMETE™ Srl, were adopted as starting material. The particles were in the range of size between 50 μm and 105 μm, and characterized by a flowability of 16 (sec/50g) in conformity to the ASTM B213-20 standard.

A DMG MORI™ Lasertec 65 3D hybrid machine with laser of wavelength 1020 nm, spot of 3000 μm, and power up to 2500 W was used for fabricating the samples in an inert argon atmosphere. A first batch of samples for tensile and fatigue testing was fabricated with the axis parallel to the building direction on an AISI 316L stainless steel platform. The adopted scanning strategy for each layer was the meander one with a 67° rotation of each layer with the respect of the previous one. The laser power was continuously decreased from 2000 W to 1100 W at increasing number of layers to prevent heat accumulation in the bulk volume. The other adopted DED parameters are summarized in Table 1.

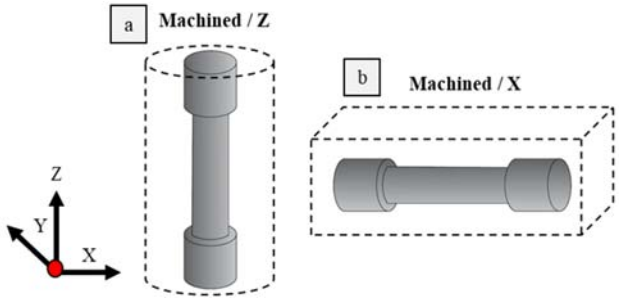

Fig. 1. AISI 316L near-net-shape samples fabricated through DED and then machined: a) with the axis parallel to the building direction Z, and b) with the axis perpendicular to the building direction Z.

A cylinder of 18 mm×18mm×150 mm size and a prism of 17 mm×160 mm×20 mm size were also fabricated through DED from which tensile and fatigue testing samples were machined with the axis parallel and perpendicular with respect to the building direction, respectively (see Figure 1). The cylinder and the prism were built on an AISI 316L stainless steel platform as well, with the process parameters detailed in Table 1. However, in this case, due to the high thermal inertia of the cylinder and the prism, the laser power was continuously decreased from 2000 W till 1500 W at increasing number of layers.

To relieve the residual stresses left by the AM process that are detrimental for the part mechanical resistance, the DED samples were heat-treated at 450°C for 1 hour in an argon-controlled atmosphere inside a Nabertherm™ LH216/13 vertical furnace, and then cooled in still air. Finally, after heat treatment, the samples were removed from the platform through Electron Discharge Machining (EDM).

The tensile and fatigue testing samples, whose geometry was in accordance with the ISO6892 and ISO1099 standards, respectively, were machined from the DED cylinder and prism on a CNC NL 1500™ Mori Seiki lathe. The machining finishing pass was carried out by adopting depth of cut 0.3 mm, cutting speed 200 m/min, and feed 0.2 mm/rev.

Table 1. DED process parameters.

Travel speed (mm/min)	Layer thickness (mm)	Hatch spacing (mm)	Powder flow rate (g/min)
1000	0.85	1.5	12

2.2. Samples characterization

Cubes of 10 mm side were extracted from the cross-section of the machined samples for metallographic investigations, then mounted in epoxy resin, and polished down to 1 µm using a diamond paste. Afterwards, they were electrolytically etched for 30 s by means of a solution of 10% of oxalic acid mixed with water.

The Sensofar™ PLu-Neox optical profiler with a 20× Nikon™ confocal objective was employed to scan the surface topography of the samples in the as-built and machined conditions. The acquired height maps with lateral dimensions of about 4 mm x 0.8 mm were subjected to form removal by subtraction of the mean cylinder. Each topography was acquired three times as well as three surface profiles were extracted to compute the roughness parameters according to the ISO 4288 standard [10], with λs filter equal to 2.5 µm, cut-off λc equal to 0.8 mm, and sampling length of 4 mm. The roughness parameter *Ra* (arithmetic mean deviation of the assessed profile) was considered as it is the parameter most commonly used to assess the surface quality of the AM parts.

2.3. Mechanical testing

Uniaxial tensile tests were carried out on a MTS™-322 hydraulic dynamometer, with maximum load of 50 KN and maximum stroke of 150 mm. The tests were carried out at a rate of 0.125 mm/s at room temperature, and repeated three times to assure the results reproducibility.

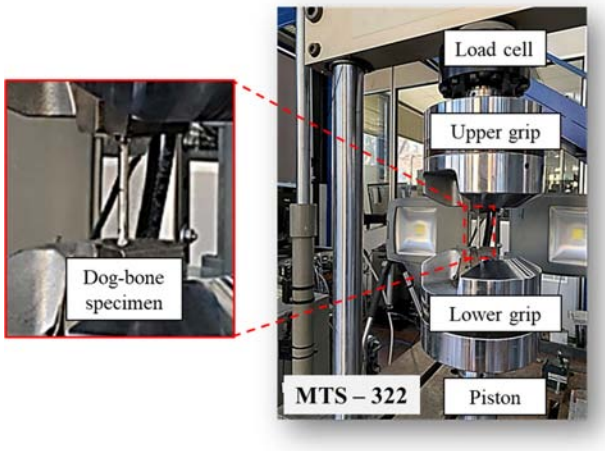

Fig. 2. Experimental equipment for mechanical testing.

Fatigue tests were carried out under a stress ratio R= -1 on the MTS™ dynamometer at room temperature. The test frequency was set equal to 10 Hz. The fatigue test was considered aborted when the whole fracture of a section occurred or the run-out criterion of $1x10^6$ load cycles was reached.

Afterwards, the fracture surfaces of the samples from both tensile and fatigue testing were inspected using a FEI™ Scanning Electron Microscope (SEM) equipped with a Secondary Electron (SE) probe. Images at both 200X and 5000X of magnification were acquired across different zones of the fracture surfaces.

Figure 2 shows a photo of the equipment used for both tensile and fatigue testing, where the specimen is mechanically fixed to the upper and lower grippers, which, in turn, are connected to the dynamometer load cell and hydraulic piston, respectively.

3. Results and discussion

3.1. Samples microstructure and surface finish

Figure 3 shows the cross-section microstructures of the machined samples. The microstructure of the *machined / Z* sample consists of a homogeneous cellular structure without any macroscopic defects, and is characterized by no evident preferential orientation (see Figure 3 (a)). Similarly, the microstructure of the *machined / X* sample appears free of macroscopic defects, nevertheless it consists of a mixture of cellular and columnar dendritic structures, with the melt pool borders that are clearly evident. Near the melt pool border, the fine cellular structure gradually converts into a combination of columnar and cellular structures (see Figure 3 (b), (c) and (d)). Such microstructure arrangement can be attributed to the predominance of conduction-based heat transfer across the heat affected zone at the melt pool borders, whereas convection dominates in the central zone of the melt pool, where the liquid metal solidifies slightly later [11]. Finally, a complex mixed convective-conductive-radiating heat transfer occurs at the edges of the laser track, where the lateral borders of the melt pool are exposed to the operating environment [11].

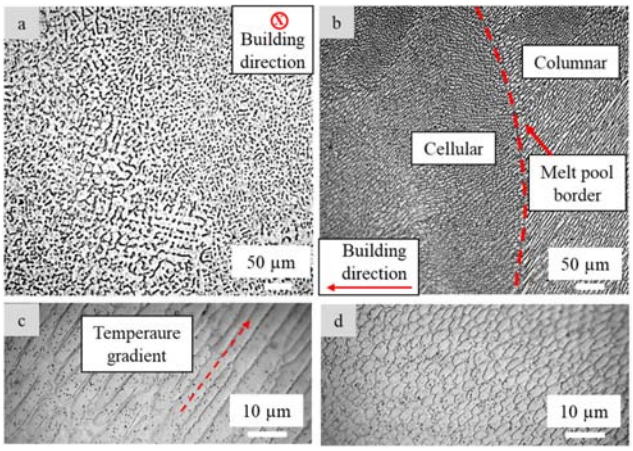

Fig. 3. Microstructure of the cross-section of the: (a) *machined / Z* sample; (b) *machined / X* sample; higher magnifications of the microstructure shown in (b) from columnar dendritic (c) to fine cellular regions (d).

Although dendritic grain growth is randomly oriented in some areas, a directional solidification is observed in particular regions where the dendrites lengthen from the melt pool borders of the melt pool towards its centre. The directional solidification gives a common microstructure orientation for laser-processed parts being the result of both high solidification rates and temperature gradients [12].

Table 2 reports the roughness values of the investigated samples. As expected, very rough surfaces characterize the as-built samples: this is attributed to both the sticking of partially melted powder particles to the surface and the stair stepping effect due to the subsequent laser tracks [13], as shown in Figure 4. On the contrary, machining contributed to drastically decrease the roughness values, leading to a surface finish improvement of 97% compared to the as-built condition, with no effect of the building direction.

Table 2. Roughness of the investigated samples.

Sample configuration	Ra (µm)
As-built / Z	17.2 ± 5.5
Machined / Z	1.63 ± 0.8
Machined / X	1.68 ± 0.1

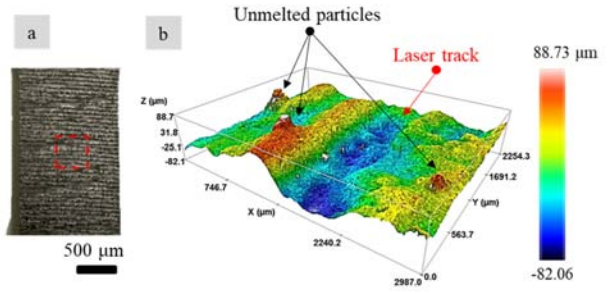

Fig. 4. (a) Surface appearance, and (b) surface texture of the *as-built / Z* sample.

3.2. Static tensile behaviour

The engineering tensile curves of the investigated specimens are reported in Figure 5. As expected, the shape of the curves is representative of a ductile behavior. For sake of clarity, the mechanical properties obtained from the curves shown in Figure 5 are summarized in Figure 6.

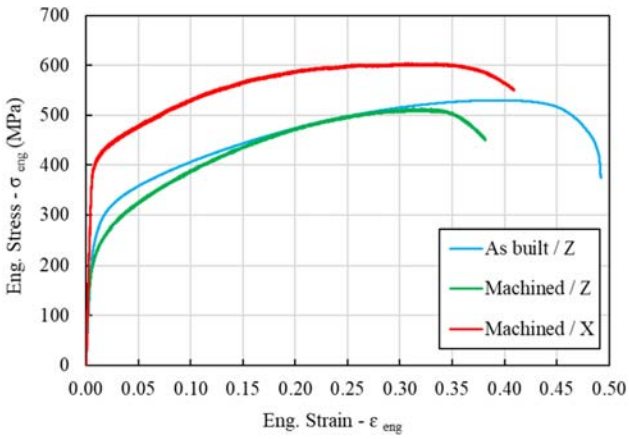

Fig. 5. Engineering stress-strain curves of the investigated samples.

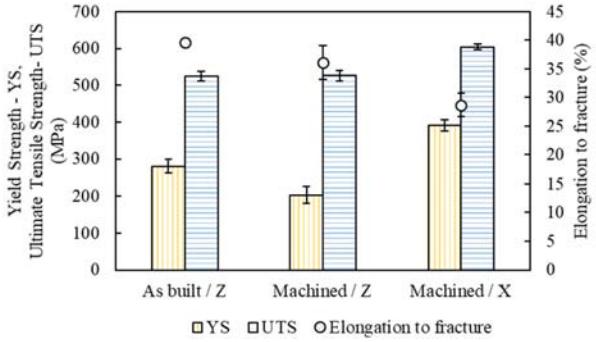

Fig. 6. Mechanical properties of the investigated samples.

It is evident that the building direction plays a primary role in determining the material static tensile behaviour since the samples machined with the axis perpendicular to the building direction present 15% higher UTS and 92% higher YS, but 26% lower elongation to fracture compared to the samples machined with the axis along the building direction. First, the accentuated grain refinement in the *machined / X* samples (see Figure 3) can be considered responsible to the mechanical strength increase. Furthermore, also the pronounced anisotropy induced by the DED process have a significant effect: as schematically depicted in Figure 7, when the specimens are machined with the axis perpendicular to the building direction, the loading direction becomes parallel to the sliced layers (see Figure 7 (a)). On the contrary, for the specimens machined with the axis parallel to the building direction, the loading direction is orthogonal to those layers (see Figure 6 (b)), thus exposing the weak metallurgical bonds between layers to the tensile state of stress [14].

A trend opposite to that of mechanical resistance was highlighted for the elongation to fracture, being higher for the *machined / Z* samples compared to the *machined / X* ones. In accordance to [14, 15], it can be explained by considering the columnar grain orientation. Actually, during the tensile failure stage, the cracks will preferentially propagate along the columnar grain boundaries, which grow orthogonally to the

scanning tracks. Thus, in the case of the *machined / X* samples, the cracks propagate faster than in the case of the *machined / Z* ones, because the columnar grain boundaries are nearly perpendicular to the loading axis, resulting in lower elongations. Finally, it is worth noting that the mechanical properties of the as-built samples (which have the axis parallel to the building direction) are pretty similar to those of the *machined / Z* ones, indicating a marginal effect of the machining operations. Actually, static failure in ductile metals occurs as a consequence of voids coalescence, being solely secondarily influenced by the surface finish [16].

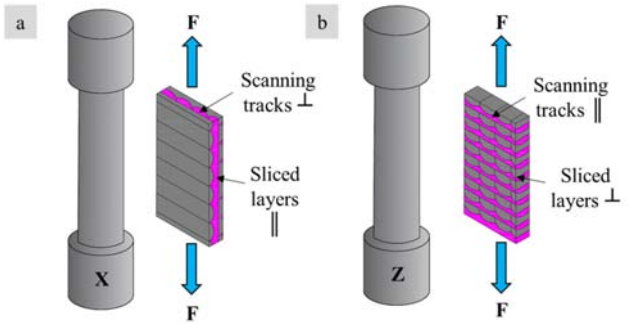

Fig. 7. Scheme of the interaction between the loading direction and orientation of the DED-induced microstructural features in the *machined / X* (a) and *machined / Z* (b) samples.

3.3. Fatigue behaviour

The results from the fatigue tests are shown in Figure 8 and summarized in Table 3. In Figure 8, the fatigue limit is plotted against the number of cycles to failure: as expected, the lowest fatigue life was found for the as-built samples, while, even if the fatigue life increased when the surfaces were machined, the samples machined with the axis parallel to the building direction showed lower fatigue life than their counterparts.

It is worth underlining that machining contributed to drastically reduce data scattering, broadening data range, contrarily to what found in [17], where more scatter in uniaxial fatigue data was observed for the machined specimens, particularly close to the endurance limit: this was attributed to the fact that fatigue cracks in the as-built specimens were observed to initiate almost always from the surface, while fatigue cracks in the machined specimens from both surface discontinuities and internal defects. On the contrary, in the present study, machining made possible the reduction of the number of cracks initiation sites, decreasing the fracture stochastic nature and contributing to the attainment of more robust fatigue data.

The fatigue behaviour of AM parts is usually associated to three distinct factors, namely the surface finish, microstructure, and orientation of defects. Figure 8 shows the fatigue limit of the investigated samples at $1*10^6$ cycles at varying the aforementioned factors.

The fatigue limit is significantly reduced when the surface roughness is the highest, namely in the case of the as-built specimens (see Figure 9 (a)). Actually, to carry out machining operations guarantees an average 131% increase in the fatigue life compared to the one of the as-built condition.

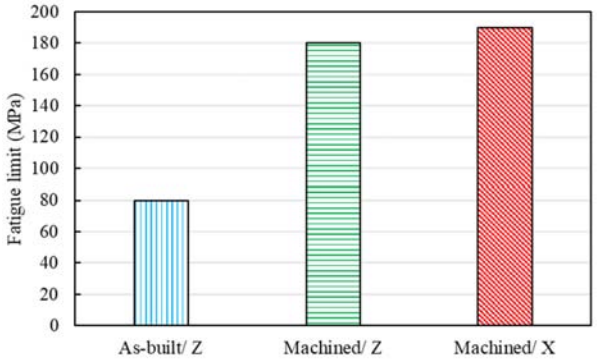

Fig. 8. Fatigue limit at $1*10^6$ cycles for the investigated samples.

Table 3. Fatigue limit versus number of cycles to failure (N_f) curve for the investigated samples.

Sample configuration	Fatigue limit (MPa)	N_f	Fatigue crack initiation site
As built	180	271616	Superficial
As built	180	541082	Superficial
As built	150	221922	Superficial
As built	120	735681	Superficial
As built	120	1008000	Run out
As built	80	1008000	Run out
As built	80	1008000	Run out
As built	80	1008000	Run out
Machined \ X	280	132677	Superficial
Machined \ X	250	270207	Superficial
Machined \ X	220	719605	Superficial
Machined \ X	190	1008000	Run out
Machined \ X	190	1008000	Run out
Machined \ X	190	1008000	Run out
Machined \ Z	210	2954	Superficial
Machined \ Z	210	5373	Superficial
Machined \ Z	195	8317	Superficial
Machined \ Z	180	1008000	Run out
Machined \ Z	180	1008000	Run out
Machined \ Z	180	1008000	Run out

This can be correlated to the removal of the external layers, which are plenty of defects, as shown in Figure 4 (a). According to [18], rougher surfaces lead to lower fatigue limits since the valleys act as stress risers, making the surfaces more prone to the nucleation of fatigue cracks. It is worth noting that several studies rightly underline that the surface roughness effect on the fatigue crack initiation cannot be adequately described by using the average roughness parameters, like *Ra* or *Sa*, alone. For example, both the areal arithmetic mean height *Sa* and areal reduced valley depth *Svk* were found not to correlate adequately with the fatigue data n in [8], whereas the skewness *Ssk* did. The Authors explained that the latter can express the probability of stress concentrations sites whereas the former only give information about the depth of possible stress concentration sites. The obsolete character of *Ra* in assessing the fatigue performances of a surface was witnessed

also in [19], where it was reported that even when the surface profile of the down-skin had a similar mean roughness of the up-skin, cracks still initiated mostly along the down-skin surface.

Nevertheless, in the present study, *Ra* was found to be sufficient for discriminating among the different fatigue properties as the surface state conditions of the as-built and machined surfaces were extremely different. Figure 9 (b) shows the effect of the columnar grain orientation with respect to the loading direction.

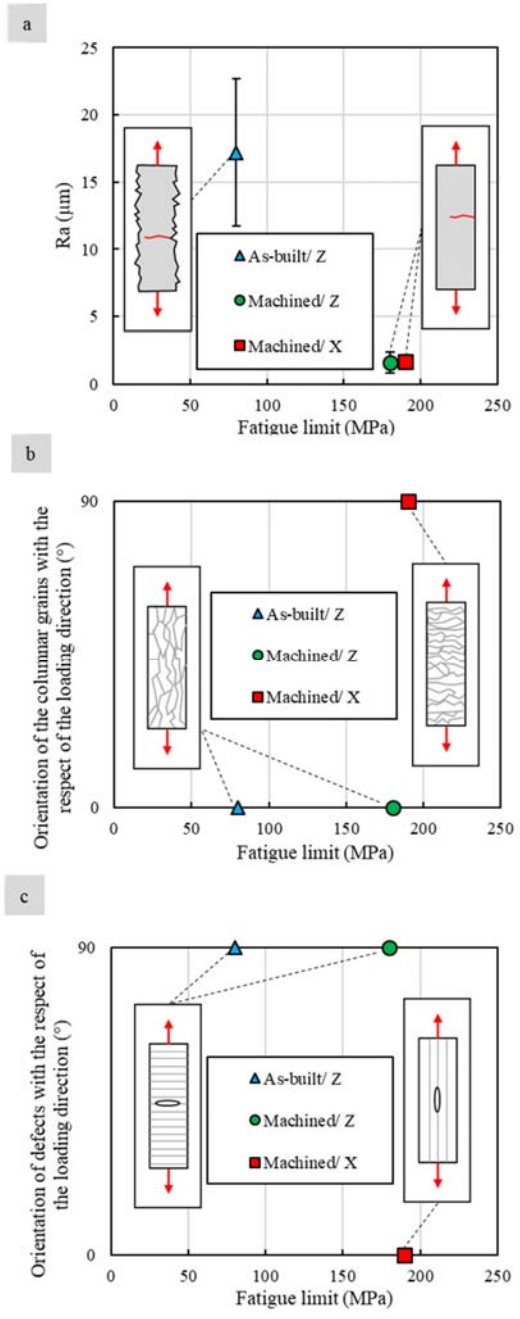

Fig. 9. Fatigue limit of the investigated samples at $1*10^6$ cycles as a function of: (a) surface roughness, (b) orientation of the columnar grains, and (c) orientation of defects with the respect of the loading direction.

When loading is parallel to the orientation of the columnar grains, the fatigue crack has to cross much more grain boundaries than when loading is normal, thus its propagation is delayed.

On the contrary, when the crack grows parallel to the building direction, the grains are elongated along the crack growth direction, therefore making the material resistance to the crack propagation lower [20]. In other words, the fatigue crack encounters a non-tortuous path when it travels along the grain boundaries and a much more tortuous one when it grows normal to the columnar grain orientation, similarly to what found for the tensile properties.

Figure 9 (c) shows the effect of the defects orientation with respect to the loading direction. Lack of Fusion (LoF) defects, namely planar regions that have not been properly fused, are a typical example of built direction-dependent internal defects. As LoFs are planar-like defects, they are most critical when loading is parallel to the building direction. Actually, in the case of the samples machined with the axis perpendicular to the building direction, the flat pores are sealed and closed during loading, whereas, in the case of the samples machined with the axis parallel, the pores start to be torn along the loading direction [21].

3.4. Fracture surfaces

Figure 10 shows the SEM images of the fracture surface of the investigated samples after tensile testing at different magnifications. In general, the fracture surface exhibits almost evenly distributed dimples, indicating fairly ductile fracture characteristics [22]. Nevertheless, a large number of voids are visible especially on the samples machined with the axis parallel to the loading direction, which are spread on the fractured surface, as highlighted in Figure 10 (a) and (c) with yellow arrows. Such voids indicate localized solidification defects (pores and cavities) induced by the DED process, as reported in several literature studies [5, 6]. Deep pores with variable diameters can be distinguished on the fracture surface, which likely evolve to larger pores during deformation. In addition, un-melted particles deriving from LoF are highlighted in Figure 10 (b), (d) and (f) with light blue circles. During tensile deformation, such discontinuities favour the crack generation, as they induce stress concentration. For this reason, they can be considered as the responsible of the different mechanical behaviour found at varying building direction (see Figure 6). Actually, samples machined with the axis perpendicular to the building direction present a homogeneous distribution of dimples with a considerably reduced density of pores, which are also of lower size. It is worth noting that, for these samples, the loading is parallel to the flat pores that tend to be closed, whereas, in the case of samples machined with the axis parallel to the building direction, the flat pores tend to be torn along the loading direction (see scheme in Figure 9 (c)).

Finally, it can be seen that the fracture surfaces are smoother for the *machined / X* samples than for the *machined / Y* ones, confirming the lower ductility of the former.

The fracture surfaces were also examined after fatigue testing. As visible in Figure 11 (a) and (c) for the *machined / Z* and *machined / X* samples, three main areas typical of fatigue

failure were identified: (i) crack initiation, (ii) crack propagation, and (iii) final fracture [5]. The propagation direction of all the cracks, which is determined on the basis of the radial lines originating from the crack initiation location, is marked with arrows. In particular, examples of initiation sites of the fatigue cracks, associated to subsurface defects that intersect the surface after the machining, are visible in Figure 11 (b), whereas Figure 11 (d) shows a cluster of un-melted particles that is likely to be the responsible of failure. As indicated in the notes of Table 3, the initiation sites of fatigue cracks were found to be close to the surfaces for all the investigated samples.

This is in accordance to what reported in [18], where, for wrought and LPBF AISI 316L stainless steel, it was found a transition of the failure location from defects close to the surface to internal ones at high stress ranges, namely for loads higher than 275 MPa. Actually, when the defects are located near the surface, it is more likely that they can readily coalesce, increasing their harmfulness.

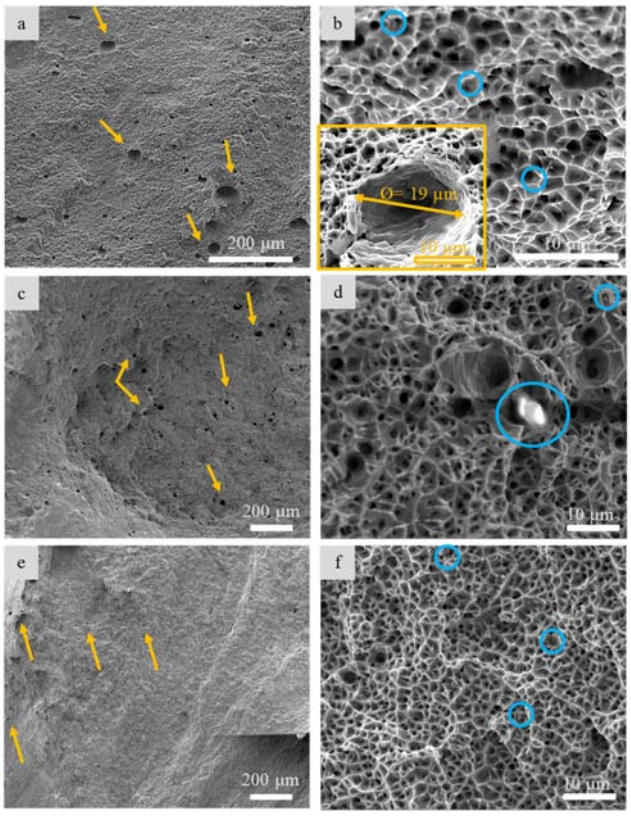

Fig. 10. Fracture surface with focus on dimples and pores of the *as-built / Z* (a, b), *machined / Z* (c, d) and *machined / X* (e, f) samples after tensile testing.

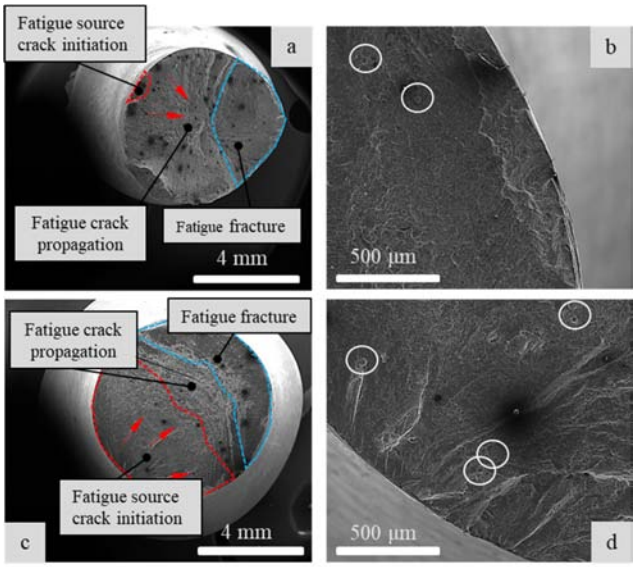

Fig. 11. Fracture surface and detail of the fatigue crack initiation site of the *machined / Z* (a, b) and *machined /X* (c, d) samples after fatigue testing.

4. Conclusions

In the present work, the effect of the building orientation and surface finish on the microstructural and mechanical properties of the AISI 316L stainless steel fabricated through DED was investigated. To this aim, three batches of DED samples were considered, namely one in the as-built condition with the axis parallel to the building direction, and the other two comprising samples machined with the axis parallel and perpendicular to the building direction. Tensile and fatigue tests were carried out on these three batches of samples to assess their mechanical properties. The fractured surfaces were finally inspected by means of SEM.

The main findings can be summarized as follows:

- The cross-section of the samples machined with the axis parallel to the building direction shows a homogeneous cellular structure, whereas the cross-section of the samples machined with the axis perpendicular to the building direction presents a finer microstructure composed of a mixture of cellular and columnar dendritic grains.
- Machining assured a 97% decrease in *Ra* compared to the as-built condition, regardless of the building direction of the investigated samples.
- The tensile behavior was mainly influenced by the building direction. Specifically, samples machined with the axis perpendicular to the building direction showed higher tensile and yield strengths than the samples machined with the axis parallel, but lower ductility. The surface finish condition was proved to give a negligible effect.
- Contrarily, the fatigue resistance was primarily affected by the surface finish conditions. Specifically, the fatigue limit increased of 131% in case of samples machined with the axis parallel to the building direction compared to the as-built ones. A further improvement

of 5% was guaranteed when testing samples machined with the axis perpendicular to the building direction.

- The fracture surface features of the tensile specimens proved that the presence of solidification-induced voids from DED played a primary role in affecting the tensile strength.
- The fracture surface features of the fatigue specimens proved that, in all cases, the fatigue cracks initiated in correspondence of the surface, highlighting the importance of the surface condition in assessing the material fatigue properties.

References

[1] Saboori A, Gallo D, Biamino S, Fino P, Lombardi M. An overview of additive manufacturing of titanium components by directed energy deposition: microstructure and mechanical properties. Appl Sci 2017; 7(9), 883.

[2] Yadollahi A, Shamsaei N, Thompson, S. M., Seely D.W. Effects of process time interval and heat treatment on the mechanical and microstructural properties of direct laser deposited 316L stainless steel. Mat Sci Eng: A 2015; 644, 171-183.

[3] Lewandowski JJ, Seifi M. Metal additive manufacturing: a review of mechanical properties. Annu Rev Mat Res 2016; 46, 151-186.

[4] Jeon J M, Park J M, Yu J H, Kim J G, Seong Y, Park S H, Kim H S. Effects of microstructure and internal defects on mechanical anisotropy and asymmetry of selective laser-melted 316L austenitic stainless steel. Mat Sci Eng: A 2019; 763:138152.

[5] Liverani E, Toschi S, Ceschini L, Fortunato A. Effect of selective laser melting (SLM) process parameters on microstructure and mechanical properties of 316L austenitic stainless steel. J Mater Process Technol 2017; 249:255-263.

[6] Yang Y, Gong Y, Qu S, Yin G, Liang C, Li P. Additive and Subtractive Hybrid Manufacturing (ASHM) of 316L Stainless Steel: Single-Track Specimens, Microstructure, and Mechanical Properties. JOM 2021; 73:759-769.

[7] Spierings AB, Starr TL, Wegener K. Fatigue performance of additive manufactured metallic parts. Rapid Prototyping J 2013; 19/2.

[8] Dumas M, Cabanettes, F., Kaminski, R., Valiorgue, F., Picot, E., Lefebvre, F., Grosjean C, Rech, J. Influence of the finish cutting operations on the fatigue performance of Ti-6Al-4V parts produced by Selective Laser Melting. Procedia CIRP 2018;71:429-434.

[9] Vilardell A.M, Krakhmalev P, Fredriksson G, Cabanettes F, Sova A, Valentin D, Bertrand P. Influence of surface topography on fatigue behavior of Ti6Al4V alloy by laser powder bed fusion. Procedia CIRP 2018;74:49-52.

[10] ISO 4288:1996 Geometrical Product Specifications (GPS)—Surface Texture: Profile method— rules and procedures for the assessment of surface texture. ISO, Geneva.

[11] Saboori A, Aversa A, Marchese G, Biamino S, Lombardi M, Fino P. Microstructure and mechanical properties of AISI 316L produced by directed energy deposition-based additive manufacturing: A review. Appl Sci, 2020; 10(9), 3310.

[12] Gäumann M., Henry S., Cleton F., Wagniere J. D., Kurz W. Epitaxial laser metal forming: analysis of microstructure formation. Mat Sci Eng: A, 1999; 271(1-2), 232-241.

[13] Svetlizky D, Das M, Zheng B, Vyatskikh A.L, Bose S, Bandyopadhyay A, Eliaz N. Directed energy deposition (DED) additive manufacturing: Physical characteristics, defects, challenges and applications. Mater Today Commun 2021; Article in Press.

[14] Simonelli M, Tse YY, Tuck C. Effect of the build orientation on the mechanical properties and fracture modes of SLM Ti–6Al–4V. Mat Sci Eng: A 2014;616:1-11.

[15] Lizzul L, Sorgato M, Bertolini R, Ghiotti A, Bruschi S. Influence of additive manufacturing-induced anisotropy on tool wear in end milling of Ti6Al4V. Tribol Int 2020; 146: 106200.

[16] Benzerga AA, Leblond JB, Needleman A, Tvergaard V. Ductile failure modeling. Int J Fract, 2016; 201(1):29-80.

[17] Wycisk E, Solbach A, Siddique S, Herzog D, Walther F, Emmelmann C. Effects of defects in laser additive manufactured Ti-6Al-4V on fatigue properties. Phys Procedia 2015 56, 371-378.

[18] Solberg K, Guan S, Razavi SMJ, Welo T, Chan KC, Berto F. Fatigue of additively manufactured 316L stainless steel: the influence of porosity and surface roughness. Fatigue Fract Eng M. 2019; 42(9):2043-2052.

[19] Pegues, J., Roach, M., Williamson, R. S., & Shamsaei, N. (2018). Surface roughness effects on the fatigue strength of additively manufactured Ti-6Al-4V. International Journal of Fatigue, 116, 543-552.

[20] Riemer A, Leuders S, Thöne M, Richard HA, Tröster T, Niendorf T. On the fatigue crack growth behavior in 316L stainless steel manufactured by selective laser melting. Eng Fract, 2014;120: 15-25.

[21] Qiu C, Ravi GA, Dance C, Ranson A, Dilworth S, Attallah M.M. Fabrication of large Ti–6Al–4V structures by direct laser deposition. J Alloys Compd 2015; 629:351-361.

[22] Simonetto E, Bertolini R, Ghiotti A, Bruschi S. Mechanical and microstructural behaviour of AA7075 aluminium alloy for sub-zero temperature sheet stamping process. Int J Mech Sci 2020; 187: 105919.